STRUCTURES OF THE TURBULENT BOUNDARY LAYER
OVER A ROD-ROUGHENED WALL

Jae Hwa Lee and Hyung Jin Sung[*]
Department of Mechanical Engineering,
KAIST
373-1 Guseong-dong, Yuseong-gu, Daejeon, 305-701, Korea
jhlee06@kaist.ac.kr, leehuiso@kaist.ac.kr, hjsung@kaist.ac.kr[*]

Seung-Hyun Lee
Korea Institute of Machinery & Materials
104 Sinseongno, Yuseong-gu, Daejeon 305-701, Korea
leehuiso@gmail.com

Kyoungyoun Kim
Department of Mechanical Engineering,
Hanbat National University
San 16-1, Duckmyoung-dong, Yuseong-gu, Daejeon 305-719, Korea
kkim@hanbat.ac.kr

ABSTRACT

Turbulent coherent structures near a rod-roughened wall are scrutinized by analyzing instantaneous flow fields obtained from direct numerical simulations (DNSs) of a turbulent boundary layer (TBL). The roughness elements used are periodically arranged two-dimensional spanwise rods, and the roughness height is k/δ=0.05 where δ is the boundary layer thickness. The Reynolds number based on the momentum thickness is varied in the range Re_θ= 300~1400. The effect of surface roughness is examined by comparing the characteristics of the TBLs over smooth and rough walls. The roughness has little effect on the vorticity fluctuations in the outer layer. Velocity-pressure gradient tensors of the transport equation for the Reynolds stresses and quadrant analysis disclose that the redistribution of turbulent kinetic energy of the rough wall is similar to that of the smooth wall, and that the introduction of rod roughness has little effect on the relative contributions of ejection and sweep motions in the outer layer. Finally, we demonstrate the existence of coherent structures in the instantaneous flow field over the rod-roughened surface to elucidate the modifications of the near-wall vortical structure.

INTRODUCTION

Townsend (1976)'s Reynolds number similarity hypothesis and subsequent extensions by Jimenez (2004) state that outside the roughness sublayer turbulent motions are independent of the surface roughness, and that the interaction between the inner and outer layers is very weak at sufficiently large values of the Reynolds number normalized by the wall shear stress. In further support of this similarity hypothesis, a number of studies have found that the outer layers of flows past smooth and rough walls were similar in terms of both mean flow and turbulent statistics, consistent with Townsend's hypothesis for three-dimensional roughness.

Results from several experimental studies of TBLs over surfaces with two-dimensional rod-roughness, however, have been contrary to the wall similarity hypothesis. For example, in experiments on TBLs over woven mesh, transverse round rod roughness elements, Krogstad & Antonia (1992, 1994) found that introduction of roughness caused significant changes of the turbulent statistics not only in the roughness sublayer but also in the outer layer and that the interaction between the inner and outer layers was non-negligible. They found that the streamwise extent of all correlations was greater for the smooth wall than that for the rough walls and that the average angle of the turbulent structure was larger over the rough walls. These experimental results oppose the notion that the outer layer of a TBL is insensitive to the surface roughness, and have led to considerable uncertainty regarding the effects of surface roughness on TBLs.

In the present study, the interaction between the inner and outer layers induced by rod roughness was examined through analysis of the DNS data of Lee & Sung (2007). The roughness was composed of two-dimensional spanwise rods with square cross-section that were periodically arranged in the streamwise direction with a pitch of λ/k=8 in which has a maximum value of form drag (Leonardi et al., 2003). To examine the outer-layer similarity and the scaling parameters, various statistics were investigated. Further, to elucidate the redistribution of turbulent kinetic energy, we examined the velocity-pressure gradient tensors in the transport equations of the Reynolds stresses. Finally, two-point correlations, conditionally averaged and instantaneous
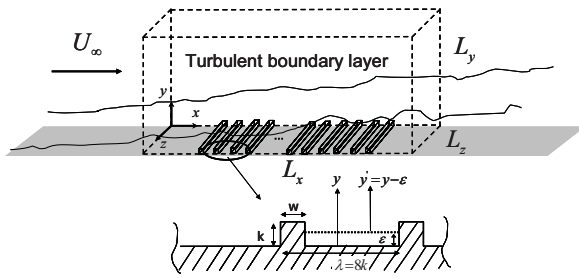
Figure 1: Schematic of computational domain.

flow fields were scrutinized to analyze the turbulent structures arising from surface roughness not only in the roughness sublayer but also in the outer layer.

NUMERICAL METHOD

For an incompressible flow, the nondimensional governing equations are

$$\frac{\partial u_i}{dt} + \frac{\partial u_i u_j}{\partial x_j} = -\frac{\partial p}{\partial x_i} + \frac{1}{Re}\frac{\partial^2 u_i}{\partial x_j \partial x_j} + f_i \qquad (1)$$

$$\frac{\partial u_i}{\partial x_i} = 0 \qquad (2)$$

where x_i are the Cartesian coordinates and u_i are the corresponding velocity components. All variables are nondimensionalized by the free-stream velocity (U_∞) and momentum thickness at the inlet (θ_{in}), and Re is the Reynolds number. The governing equations are integrated in time using the fractional step method with the implicit velocity decoupling procedure proposed by Kim et al. (2002). In the present study, the immersed boundary method is used to describe the roughness elements with Cartesian coordinates and a rectangular domain (Kim et al., 2001). The discrete-time momentum forcing f_i is calculated explicitly in time to satisfy the no-slip condition at the immersed boundary using the previous velocity field near the forcing point.

Figure 1 shows a schematic of the computational domain and the two-dimensional rod roughness used in the present study. The notational convention adopted is that x, y and z denote the streamwise, vertical and spanwise coordinates and u, v and w denote the velocity components of (x, y, z), respectively. The computational domain in each direction (L_x x L_y x L_z) is $768\theta_{in}$ x $60\theta_{in}$ x $80\theta_{in}$, where the corresponding mesh size is 2049 x 150 x 257. Time-dependent turbulent inflow data are provided at the inlet based on the method of Lund et al. (1998). A convective boundary condition at the exit has the form $(\partial u/\partial t)+c(\partial u/\partial x)=0$, where c is the local bulk velocity. The no-slip boundary condition is imposed at the solid wall, and the boundary conditions on the top surface of the computational domain are $u= U_\infty$ and $\partial v/\partial y=\partial w/\partial y=0$. A periodic boundary condition is applied in the spanwise direction. Non-uniform hyperbolic tangent grid distributions are employed in y direction and a uniform grid distribution in both the x and z directions. The mesh resolutions are Δx^+=6.0, Δy_{min}^+=0.2 and Δz^+=5.0. To avoid generating a rough-wall inflow, the first rod is placed $80\theta_{in}$ downstream
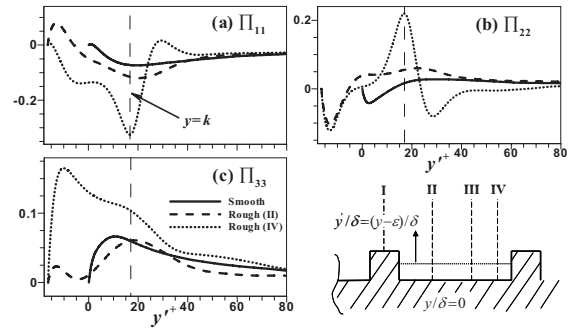
Figure 2: Velocity-pressure gradient tensors in the inner coordinates, normalized by u_τ^4/ν.

from the inlet, and the surface condition changes abruptly from smooth to rough at this location. The virtual origin (ϵ), which is the centroid of the momentum of the forces acting on the rod roughness, is used for the wall-normal distance from the wall. Details regarding the numerical algorithm can be found in Lee & Sung (2007).

TURBULENT STATISTICS

Introduction of rod roughness elements onto a smooth surface significantly affects the turbulent flow structures, leading to very high turbulent intensities in the vicinity of the wall. This near-wall region, which is known as the roughness sublayer, is generally assumed to have a height of 2~5 times the roughness height. The limit of the roughness sublayer is defined as the point at which the turbulence statistics become spatially homogeneous (Bhaganagar et al., 2004). Schultz & Flack (2005) defined the roughness sublayer as the distance from the wall beyond which the roughness no longer has an influence on the turbulence statistics. Jimenez (2004) suggested that when δ/k is larger than 40, wall similarity can be expected and the extent of the roughness sublayer is about $5k$. Schultz & Flack (2005) proposed that k_s (the effective sand-grain roughness height) is a better representative length scale for defining the extent of the roughness sublayer compared to k, because of a common measure of the influence of the roughness. In the present study, the rod roughness has a height of δ/k=20, which is larger than the criterion of Jimenez (2004). The depth of the roughness sublayer in the present study, $5k$, is estimated to be about 0.25δ ($5k_s$=1.59δ).

Previously, Lee & Sung (2007) showed that although introduction of surface roughness elements affects the turbulent Reynolds stresses throughout the boundary layer when normalized by the friction velocity, good similarity is observed for the Reynolds anisotropic tensor in the outer layer without normalization by the friction velocity. This indicates that although the increased production of turbulent kinetic energy in the vicinity of the rough wall causes an increase in the Reynolds stresses, it makes no significant contribution to the relative magnitude of the Reynolds stresses. The turbulent energy is redistributed in a manner similar to that observed for a smooth wall. To better comprehend the redistribution of turbulent energy, velocity-pressure gradient tensors in the Reynolds stress budget equation are scrutinized in detail. Although the pressure
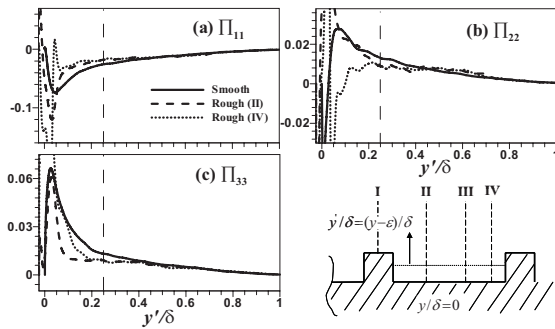
Figure 3: Velocity-pressure gradient tensors in the outer coordinates.

Figure 4: Vorticity fluctuations in the outer coordinates, normalized by u_τ^2.

term associated with the redistribution of energy is not measurable in experimental studies, its effect is important close to the wall. The velocity-pressure gradient tensors relevant to the system examined in the present study is written as

$$\Pi_{ij} = -\left\langle u_i \frac{\partial p}{\partial x_j} + u_j \frac{\partial p}{\partial x_i} \right\rangle \tag{3}$$

where the indices i, j are 1, 2, or 3 for the streamwise, wall-normal and spanwise directions, respectively. The profiles of the pressure-strain redistribution tensors are displayed in Fig. 2. All quantities are normalized by u_τ^4/ν. Figure 2(d) indicates four selected locations, denoted by I-IV. Section I is located at the center of the roughness crest (s=0.5). Section II is located at the focal point of the primary recirculation zone downstream of the roughness element (s=3.5) and Section III is located at the saddle-point between the two recirculation zones (s=6.25). Finally, Section IV is located at the focal point of the second recirculation zone (s=7.5). In each plot, a vertical dashed line is used to mark the roughness crest (y=k). The profiles of the pressure-strain redistribution in the roughness sublayer differ significantly between the smooth and rough wall systems. Within the cavity and very near the bottom wall, turbulent kinetic energy is transferred from the vertical direction to the streamwise direction at position II and to the spanwise direction at position IV. Furthermore, above the roughness crest, turbulent energy is transferred from the streamwise direction to the vertical and spanwise directions. Near the leading edge (position IV), this energy transfer is very large and constitutes the main energy source of wall-normal and spanwise velocity fluctuations, as shown in the Reynolds anisotropic tensor. These results are consistent with those for channel flow reported by Ashrafian & Andersson (2006). However, no discernible difference in the outer coordinates (Fig. 3) is observed between the rough-wall and smooth-wall TBLs above y/δ=0.45 ($y\sim9k$ and $y\sim1.5k_s$), indicating that the redistribution of turbulent kinetic energy in the outer layer is similar in the systems with smooth and rough walls. This finding supports the conjecture of Lee & Sung (2007) that rod roughness does not significantly affect anisotropy tensors in the outer layer.

Figure 4 shows the distributions of the r.m.s. vorticity fluctuations normalized by the friction velocity for the rough and smooth walls in the outer coordinates. Above the region y/δ=0.55 ($y\sim11k$ and $y\sim2k_s$), the vorticity fluctuations of the rough and smooth walls collapse well and attain the same magnitude. This indicates that above the roughness region, the small-scale structures of the vortical motions are almost the same over the rough and smooth walls. In the roughness sublayer, however, the presence of the rod roughness causes the maximum values of the three components to be smaller for the rough wall than for the smooth wall.
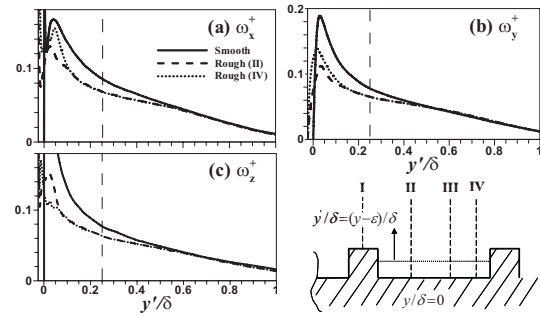
Figures 5(a) and (b) show the contributions of the Q2 and Q4 events, respectively, to the Reynolds shear stress, normalized by the local mean Reynolds shear stress. To inspect the turbulent structure in the vicinity of the rough wall, two locations over the rough wall (II and IV) and one over the smooth wall are compared. Good agreement is observed between the smooth and rough walls for both the Q2 and Q4 events above y/δ=0.16 ($y\sim3k$ and $y\sim k_s$), which is consistent with the Reynolds anisotropic tensors. These results are consistent with those of Schultz & Flack (2007), which showed outer layer similarity for three-dimensional roughness in the form of a honed pipe by investigating the percentage contributions from the ejection and sweep events. In the present study, despite the use of a roughness height of δ/k=20 (δ/k_s=3.2), good wall similarity is observed for the contributions of the Q2 and Q4 events in the outer layer for the smooth and rough walls when these variables are normalized by the local Reynolds shear stress. However, when scaled by the friction velocity, the contributions of the Q2 and Q4 events to the Reynolds shear stress in the outer layer differ markedly between the smooth and rough-walled systems (not shown here). This behavior is similar to that found in other experiments on TBLs over rough walls. Krogstad & Antonia (1992) observed that for most of the boundary layer, the magnitudes of the Q2 and Q4 events are larger across the whole boundary layer for a woven mesh roughness of roughness height δ/k_s=15 than for the smooth wall. These findings indicate that although the magnitudes of the Q2 and Q4 events vary not only in the roughness sublayer but also in the outer layer, the relative contributions from ejection and sweep motions in the outer layer are similar for the smooth and rough-walled systems, as was observed for the Reynolds anisotropic tensor.
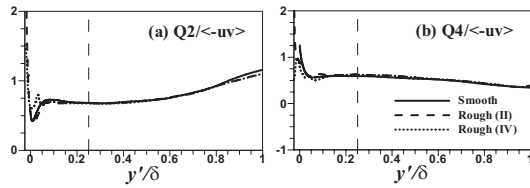
Figure 5: Quadrant analysis in the outer coordinates, normalized by local mean Reynolds shear stress.

Figure 6: Visualization of vortical structures near the roughness sublayer. (a) instantaneous velocity-vector plot of (u,v) near the roughness sublayer, (b) instantaneous velocity-vector field with the reference frame velocity $U_f=0.4U_\infty$, iso-contour represents the swirling strength.

TURBULENT STRUCTURES

The presence of rod roughness on the surface induces substantial changes in the flow field not only within the cavities between consecutive rods, but also in a certain layer above the crests of the rods. These effects can be attributed to the vigorous ejection and sweep motions that occur in these systems, as observed in the quadrant analysis. The instantaneous flow fields within the roughness sublayer reveal the characteristics of the turbulent structure over the rough wall. Figure 6 shows a visualization of the vortical structures near the roughness sublayer. The Galilean decomposition technique is applied to instantaneous velocity vectors with the reference velocity $U_f=0.4U_\infty$ in Fig. 6(b) (Adrian et al., 2000). Vortical structures are identified by a positive value of the swirling strength λ_{ci} (Zhou et al., 1999). Figure 6(a) shows instantaneous velocity vectors (u,v) in the (x,y)-plane through the middle of the spanwise computational domain, while Fig. 6(b) shows the corresponding vector field of velocity fluctuations and iso-contours of vortical structures with the reference velocity $U_f=0.4U_\infty$ in the roughness sublayer. A pattern of nearly circular streamlines that coincides with the concentrated vorticity can be discerned in Fig. 6(a). The regions colored light grey also contain concentrated vorticity, but their vector pattern shows only a faint circular signature because of different convection velocities. These vortices are inclined at approximately 25~26° with respect to the downstream direction. In similar experiments, Volino et al. (2007) found angles of $13.2 \pm 2.5°$ and $15.8 \pm 3.3°$ for smooth and rough walls, respectively. A time sequence of the instantaneous flow fields shows highly disrupted vortical structures above the roughness crest, and that these structures recover rapidly with moving upwards away from the rod roughness and attain a coherence similar to that observed for the smooth wall.

Previously, instantaneous flow fields have been used to show how turbulent structures are influenced by rod roughness within the boundary layer. However, a question remains as to whether the spatial and statistical properties of the coherent structures are similar in the outer layer of rough and smooth walls. Several previous experimental and numerical studies have elucidated the spatial characteristics of the flow past a rough wall. Using two-point correlations, Krogstad & Antonia (1994) found that introduction of a woven mesh with $\delta/k_s=15$ onto a smooth wall caused a substantial decrease of the average extent of the streamwise two-point correlations both in the roughness sublayer and in the outer layer. On the other hand, recent laser-Doppler velocimetry (LDV) and particle image velocimetry (PIV) measurements over a woven mesh surface ($\delta/k=71$) and over a smooth wall by Volino et al. (2007) showed excellent agreement, both qualitatively and quantitatively, between the turbulent structures in the spectra of the fluctuating velocity components, swirl strength, and two-point auto- and cross-correlations of the fluctuating velocity and swirl.
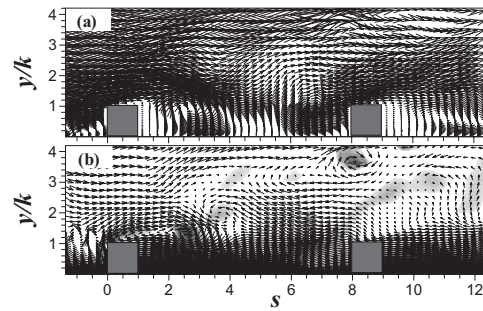
In the present study, we examined the auto-correlation of velocity fluctuations to investigate the spatial character over the rough wall. The two-point correlation of velocity fluctuations is defined as:

$$R_{ij}(\Delta x, y', \Delta z; x_{ref}, y_{ref}) =$$
$$\frac{\langle u_i(x_{ref}, y_{ref}, z) u_j(x_{ref}+\Delta x, y', z+\Delta z)\rangle}{\sqrt{\langle u_i^2(x_{ref}, y_{ref})\rangle}\sqrt{\langle u_j^2(x_{ref}+\Delta x, y')\rangle}}, \quad i,j=1,2,3 \quad (4)$$

where x_{ref} and y_{ref} denote the reference positions in the streamwise and wall-normal directions and the subscripts i and j are the corresponding Cartesian coordinates. Figure 7 shows contour plots of the two-point correlations of the streamwise velocity fluctuations R_{uu} at both $y_{ref}^+=50$ and $y_{ref}/\delta=0.5$ in the (x,y)-plane. The contours of constant correlation magnitude are roughly elliptical in shape with the major axis tilted at an angle to the streamwise direction. The streamwise two-point correlations for the smooth and rough walls in the outer layer are in excellent agreement, as shown in Figs. 7 (c-d). The mean inclination angle of $R_{uu}=0.3$ is about 11~12° and the shape of the contours is almost the same. In the roughness sublayer, however, marked differences are observed between the smooth- and rough-wall boundary layers. The contour of two-point correlations $R_{uu}=0.3$ indicates that the average extent of the streamwise two-point correlation decreases and the angle of inclination of R_{uu} significantly increases due to the rod roughness. The contour of R_{uu} is inclined at an average angle of about 26° with respect to the rough wall compared to about 13~14° with respect to the smooth wall. In the experimental study of Krogstad & Antonia (1994), the mean inclination angle of the $R_{uu}=0.3$ contour had an average value of about 10° for the smooth wall and a much larger value of about 38° for the rough wall. In the DNS studies of the turbulent channel flow over rough wall, Coceal et al. (2007) found that the mean angle with respect to the wall decreased sharply with height from 21.6° at the top of the roughness ($y=k$) to 14.4° at $y=1.5k$, then decreased more

Sixth International Symposium on Turbulence and Shear Flow Phenomena
Seoul, Korea, 22-24 June 2009
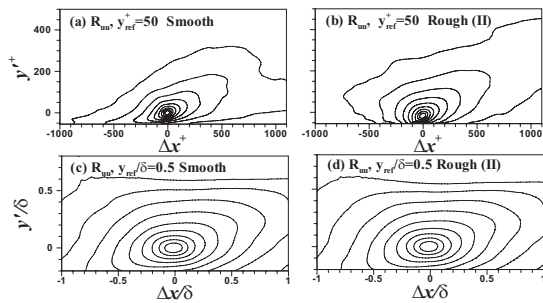
Figure 7: Contours of R_{uu} in the (x,y)-plane, contour magnitudes of R_{uu} vary from 0.1 to 0.9, (a) smooth wall $y^+=50$, (b) rough wall $y^+=50$, (c) smooth wall $y/\delta=0.5$, (d) rough wall $y/\delta=0.5$.

slowly thereafter to a value of 12.2° at $y=2.75k$. Leonardi et al. (2004) showed that a decreased streamwise coherence, relative to the smooth wall, is observed for rough wall and the inclination is increased.

Both the quadrant analysis results and the two-point correlation data provide evidence of organized motions in the TBL above the rough wall. In the present study, since we are interested in changes in the turbulent structures induced by introducing rod roughness onto a smooth wall, it is useful to study the effects of three-dimensional flow structures associated with Reynolds shear stress-producing events. To better comprehend the modification of the flow structures, we examined the conditionally averaged flow field around these structures. We approximate the conditionally averaged flow field by linear stochastic estimation (Adrian, 1996). The accuracy of linear stochastic estimation as an approximation to the conditional average has been reported elsewhere.

Figures 8 and 9 show the isosurfaces of λ_{ci} computed from the estimated velocity field for the Reynolds stress maximizing the Q2 event specified at different y locations ($y^+=50$ and $y/\delta=0.5$) over rough and smooth walls. To exclude the mean shear effects induced by the surface roughness, the velocity fluctuation components are used to obtain the swirling strength of the vortical structure. Though not shown here, the results for the Q4 event are similar to those of the Q2 event. In the turbulent boundary layer over the smooth wall, it is well known that flow structures associated with the Q2 event are a counter-rotating pair of streamwise vortices very near the wall that induces ejection motion between the vortices, and hairpin structures further away from the wall (Adrian et al., 2000). Over the rough wall, the streamwise vortical structures are significantly affected near the wall, as shown in Fig. 8. In the roughness sublayer at $y^+=50$, the streamwise length scale is shortened and the inclination angle is increased due to the surface roughness. The DNS study of channel flow by Ashrafian et al. (2004) yielded similar results; specifically, they found that although the mean flow and the turbulence statistics are dramatically affected by the rods within the roughness sublayer, streamwise vortical structures can be observed above the rods in the rod-roughened channel flow. The amount of flow structures might interact with the roughness element. Moreover, the distributions of velocity vectors associated with maximizing the Q2 event in the (x,y) and
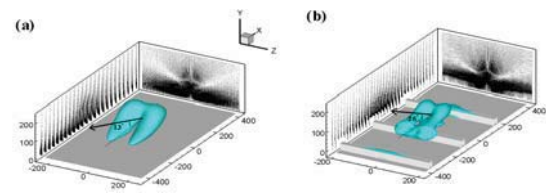
Figure 8: Vortical structure and velocity vectors extracted from a Q2 event maximizing the Reynolds shear stress at $y^+=50$. Three-dimensional structures represent iso-surfaces of λ_{ci}, and the contour level is equal to 30% of the maximum. The velocity vectors show the in-plane perturbation velocities. The (x,y)-cross-sections are located on the middle of the computational domain and cut through the hairpin head. The (y,z)-cross-sections are at $x^+=0$. (a) smooth wall, (b) rough wall.

(x,z)-planes are disturbed by the reduced damping of the wall-normal velocity fluctuations close to the rough wall and by the break-up of structures. Compared to the smooth wall, the vector fields related to ejection motions over the rough wall are widely distributed along the wall-normal direction and the magnitude of the Q2 event is larger. Lee & Sung (2007) observed a very large positive peak of the velocity triple product for the rough wall system, indicative of very strong ejection events. Above the roughness sublayer, however, the characteristics of the velocity field and swirling strength of the rough wall are similar to those of the smooth wall. This is consistent with the experimental data of Volino et al. (2007), who demonstrated that the two-point correlations of various quantities and average angles of maximum correlation are in quantitative agreement between the smooth and rough wall systems in the region above the roughness sublayer. These findings indicate that turbulent vortices producing Reynolds stress in the outer layer of the rough wall system have almost the same geometrical shape as those in the smooth wall system.

CONCLUSIONS

Instantaneous flow fields of the DNS of Lee & Sung (2007) were used to elucidate the effects of surface roughness on a TBL. The roughness elements employed were periodically arranged two-dimensional spanwise rods, and the roughness height was $k/\delta=0.05$. The Reynolds number based on the momentum thickness is $Re_\theta=1351$ for rough wall and $Re_\theta=1098$ for smooth wall, respectively.

We found that introduction of these roughness elements onto the smooth wall affected the Reynolds stresses throughout the entire boundary layer when normalized by the friction velocity, but that vorticity fluctuations in the outer layer were only mildly affected. These findings indicated that the structure of small-scale turbulence characteristics such as vorticity fluctuations is similar for smooth and rough walls, whereas turbulent stresses acting over a large scale are affected in the outer layer. Inspection of the velocity-pressure gradient tensors, which are independent of the estimated friction velocity, disclosed that despite the increased Reynolds stresses in the vicinity of the rough wall compared to the smooth wall, the redistribution
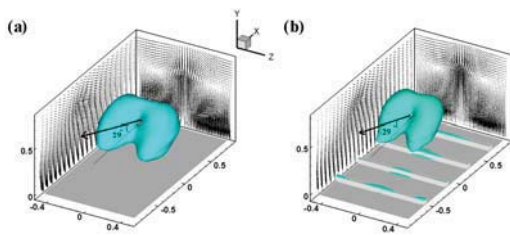
Figure 9: Vortical structure and velocity vectors extracted from a Q2 event maximizing the Reynolds shear stress at y/δ=0.5. Other conditions are the same as in Fig. 8.

of turbulent energy over the rough wall is very similar to that of the smooth wall in the outer layer. Consistent with this, while the Q2 and Q4 events normalized by the friction velocity exhibited a lack of wall similarity, good wall similarity for the Q2 and Q4 events was observed in the outer layer when normalized by the local mean Reynolds shear stress. These findings demonstrate that the outer-layer similarity between rough and smooth walls depends on the scaling parameter and turbulent statistics used. Although the magnitudes of the turbulent intensities are larger for the rough wall than for the smooth wall, the relative magnitudes of the Q2 and Q4 events were similar for the rough and smooth walls in the outer layer. Conditional averaging was carried out to investigate the turbulent vortices associated with the production of Reynolds shear stress by using linear stochastic estimation. The conditionally averaged flow fields for the Reynolds-stress-maximizing Q2/Q4 events showed that the near-wall vortical structures were strongly lifted up and shortened in the streamwise direction by the surface roughness. The ejection motion was strongly induced by the blockage effect of the surface roughness, and the surface rods affected not only the magnitude but also the distribution of the swirling strength. However, compared to the smooth-wall TBL, no discernible structural differences exist in the outer layer. These findings illustrate that introduction of surface roughness elements onto the smooth surface did not significantly affect the turbulent vortices producing Reynolds stresses in the outer layer.

ACKNOWLEDGEMENT

REFERENCES

Adrian, R. J., 1996, "Stochastic estimation of the structure of turbulent fields," *In Eddy Structure Identification (ed. Bonnet JP)*, Springer, 145-196.

Adrian, R. J., Meinhart, C. D., and Tomkins, C. D., 2000, "Vortex organization in the outer region of the turbulent boundary layer," *J. Fluid Mech* 422, 1-54.

Ashrafian, A., and Andersson, H. I., 2006, "Roughness effects in turbulent channel flow," *Progress in Computational Fluid Dynamics* 6, 1-20.

Ashrafian, A., Andersson, H. I., and Manhart, M., 2004, "DNS of turbulent flow in a rod-roughened channel," *Int J Heat Fluid Flow* 25, 373-383.

Bhaganagar, K., Kim, J., and Coleman, G., 2004, "Effect of roughness on wall-bounded turbulence," *Flow Turbulence Combustion* 72, 463-492.

Coceal, O., Dobre, A., and Thomas, T. G., 2007, "Structure of turbulent flow over regular arrays of cubical roughness," *J. Fluid Mech* 589, 375-409.

Jimenez, J., 2004, "Turbulent flows over rough walls," *Annu Rev Fluid Mech* 36, 173-196.

Kim, J., Kim, D., and Choi, H., 2001, "An immersed boundary finite-volume method for simulations of flow in complex geometries," *J. Comput. Phys* 171, 132-150.

Kim, K., Baek, S. –J., and Sung, H. J., 2002, "An implicit velocity decoupling procedure for the incompressible Navier-Stokes equations," *Intl J Numer Meth Fluids* 38, 125-138.

Krogstad, P. –Å., and Antonia, R. A., 1992, "Comparison between rough- and smooth-wall turbulent boundary layers," *J. Fluid Mech* 245, 599-617.

Krogstad, P.-Å., and Antonia, R. A., 1994, "Structure of turbulent boundary layers on smooth and rough walls," *J. Fluid Mech* 277, 1-21.

Lee, S. –H., and Sung, H. J., 2007, "Direct numerical simulation of turbulent boundary layer over a rod-roughened wall," *J. Fluid Mech* 584, 125-146.

Leonardi, S., Orlandi, O., Djenidi, L., and Antonia, R. A., 2004, "Structure of turbulent channel flow with square bars on one wall," *Int J Heat Fluid Flow* 25, 384-392.

Leonardi, S., Orlandi, P., Smalley, R. J., Djenidi, L., and Antonia, R. A., 2003, "Direct numerical simulations of turbulent channel flow with transverse square bars on one wall," *J. Fluid Mech* 491, 229-238.

Lund, T. S., Wu, X., and Squires, K. D., 1998, "Generation of turbulent inflow data for spatially-developing boundary layer simulation," *J. Comput. Phys* 140, 233-258.

Schultz, M. P., and Flack, K. A., 2005, "Outer layer similarity in fully rough turbulent boundary layers," *Exp Fluids* 38, 328-340.

Schultz, M. P., and Flack, K. A., 2007, "The rough-wall turbulent boundary layer from the hydraulically smooth to the fully rough regime," *J. Fluid Mech* 580, 381-405.

Townsend, A. A., 1976, "The structure of Turbulent Shear Flow," *2nd ed. Cambridge University Press*, Cambridge, UK.

Volino, R. J., Schultz, M. P., and Flack, K. A., 2007, "Turbulence structure in rough- and smooth-wall boundary layers," *J. Fluid Mech* 592, 263-293.

Zhou, J., Adrian, R. J., Balachandar, S., and Kendall, T. M., 1999, "Mechanisms for generating coherent packets of hairpin vortices," *J. Fluid Mech* 387, 353-396.